

COVER PAGE

Document downloaded by @DAEL

Sun Nov 15 00:34:36 2026
For personal use

When automatic English translation is provided, only the original document is authentic.
The EAA cannot be held responsible of any translation error

Bibliographical reference

Characterization of Target Spheres for Broad-Band Calibration of Acoustic Systems, Halvor Hobaek and Tonje Nesse Forland, Acta Acustica **vol. 99** (Number 3), 2013, pp. 465-476

DOI
https://doi.org/10.3813/AAA.918627

Acta Acustica united with Acustica
Vol. 99 (2013) 465 – 476

DOI 10.3813/AAA.918627

Characterization of Target Spheres for Broad-Band Calibration of Acoustic Systems

Halvor Hobæk, Tonje Nesse Forland
Department of Physics and Technology, University of Bergen, Allégt 55, 5007 Bergen, Norway.
halvor.hobak@ift.uib.no

Summary
Sonars and echo sounders are frequently calibrated using echoes from spheres of copper or tungsten carbide at spot frequencies in narrow frequency bands. Modern transducers require methods for calibration of broader frequency bands. In this paper a method is presented and applied to two commercial transducers centred at 120 kHz and 200 kHz, respectively. A demand for accurately known parameters of the calibration spheres was recognized. A method for determining compressional and shear wave speeds in such spheres is demonstrated, using dominant dips in the echo spectra in combination with computed form functions, and an inversion scheme based on the Nelder-Mead simplex algorithm. The wave speeds of 4 tungsten carbide spheres and 9 copper spheres were determined. The copper spheres ageing from 30 years to recent were examined for possible evidence of age effects, and none were found. Suspending the spheres in mono filament nylon cages requires soaking in water for at least 5 hours to obtain stable echoes. This time is not affected by dipping the spheres in detergent solutions. Finally, an approximate method to find the magnitude of the transducer transfer functions is demonstrated.

PACS no. 43.30.Xm, 43.58.Vb, 43.30.Yj

1. Introduction

Backscattering of sound from elastic spheres is commonly applied for calibration of echo sounders and sonars, based on a precise knowledge of the scattering properties of the spheres. Since the last 30 years "standard" spheres for such calibration has mainly been made of copper (Cu), or tungsten carbide (WC) with 6 % binder of cobalt [1, 2]. Electro-grade copper is available to a high degree of purity (99.9 %) so that material properties of such spheres ought to be constant and independent of manufacturer. Also WC has been assumed to have very predictable properties, and is more resistant to corrosion than copper. Up to recent times the need for calibration of echo sounders has been limited to narrow frequency bands, and accuracy of ±0.1 dB has been claimed [1]. Recently a need for measuring scattering over a wider frequency range met with problems due to mismatch of dips in the measured spectra from the standard spheres and form functions computed using nominal parameters for the spheres. To this end a separate study of standard spheres were undertaken in order to provide more accurate sphere parameters. As a second issue it was questioned whether ageing of copper with time after production, as experienced for example in water copper pipes, would affect the acoustical scattering properties of copper spheres.

Received 22 January 2013,
accepted 29 March 2013.

Scattering from spheres has received a substantial attention in the literature. The first theoretical study of sound scattering from elastic spheres was given by Faran [3], and dealt with incident plane compressional waves on an elastic, isotropic and homogeneous sphere immersed in a uniform, inviscid fluid. An excellent review of scattering from elastic bodies in general is given by Hackman [4]. Neubauer *et al.* [5] were probably the first to use the minima ("big dips") in the frequency spectra from backscattered reflection from aluminium and WC spheres to determine the compressional and shear wave speeds. MacLennan and Dunn [6] used the same method on WC spheres using linear interpolation between pairs of big dips. In the present work this method has been refined using several big dips and inversion based on a simplex algorithm.

At the introduction of composite ceramic transducers wider frequency ranges became available, and several recent papers address methods for calibrating wide band systems. Dragonette *et al.* [7] used signals so short that the first echo could be separated from the elastic responses occurring later. This echo represents geometrical reflection which has an approximately constant reflectivity at high frequencies. Stanton and Chu [8] used a similar method, separating the geometrical echo with matched filtering of a chirped transmit pulse. Foote *et al.* [9] reported broad band calibration of an echo sounding system spanning a range of 7 octaves (25 kHz to 3.2 MHz) using WC spheres of diameter 10 and 20 mm. Atkins *et al.* [10] suggest to use multiple spheres simultaneously, dimensioned such that their big dips do not overlap, and combining the regions

© S. Hirzel Verlag · EAA

Document downloaded by @DAEL, 2026-11-15 00:34:39 - personal use only

between the dips for calibration. A similar approach was used by Ona *et al.* [11]. Islas-Cital *et al.* [12] employed a linear chirp and pulse compression to obtain time-domain response of the echo, allowing calibration of both amplitude and phase over a frequency range 60-120 kHz. In the present work a somewhat simpler procedure is used, focusing only on amplitude calibration.

Institute of Marine Research (IMR) in Bergen, Norway, kindly supplied us with a set of WC spheres of diameters 22, 38.1, 75 and 84 mm diameter, and Cu standard spheres of 30 and 60 mm diameter. The measurements were made in a laboratory tank with tap water at room temperature. Instead of ordinary echo sounder equipment standard laboratory instruments were used, in order to have full control of the measurement conditions.

The organization of the paper is as follows. A short theory section is included in order to clarify the calibration procedure. The experiment section describes the set up, the measurement procedure (including a discussion of suspension) and the method used for inversion. The results section covers the WC spheres and the Cu spheres separately. A separate section shows examples on broad band calibration using two WC spheres, followed by a section on transducer response functions. Discussion and conclusions terminate the paper.

2. Theory of calibration

The purpose of calibration is to obtain information about instrumental parameters like transducer and amplifier response of an acoustical system. In the following the same transducer is used as transmitter and receiver (monostatic) and the target is assumed to be located on the acoustic axis of the transducer, in its far field (the transducer also in the farfield of the target). Absorption in the medium is ignored, but can be easily included. The calibration is relative, in the sense that one may find the target strength of a target, as opposed to absolute calibration where the transmitting and receiving sensitivity of the transducer relates pressure amplitude and voltage. Thus, the principle rests on comparing the reflected signal of a target to that of a target with known scattering cross section, i.e. a calibration sphere.

The (differential) backscattering cross section is commonly defined as

$$\sigma_{bs} = r^2 \frac{I_{bs}}{I_i}, \tag{1}$$

where I_{bs} is the received backscattered intensity, I_i is the incident intensity at the target and r distance between transducer and target. Target strength is defined as

$$TS = 10 \log_{10} \left(\frac{\sigma_{bs}}{r_0^2} \right), \tag{2}$$

where r_0 is a reference distance (1 m). If $\mathcal{R}$ is the reflection function of the target the scattered pressure at the transducer is $p_s = (r_0/r) p_i * \mathcal{R}$, where p_i is the incident pressure at the target and $*$ denotes convolution.

Since the reflection function in general is frequency dependent, it is instructive to present the analysis in the frequency domain. The amplitude spectrum of the received electrical signal $|V_m|$ may be expressed as

$$|V_m| = |V_t| \cdot |g_1| \cdot |g_2| \cdot \left(\frac{r_0}{r} \right)^2 \cdot |\hat{\mathcal{R}}| \equiv \Phi \cdot |\hat{\mathcal{R}}|, \tag{3}$$

where $|V_t|$ is the amplitude spectrum of the electric signal input to the transducer as transmitter, g_1 and g_2 the transfer function of the transducer as transmitter and receiver, respectively, and $\hat{\mathcal{R}}$ is the reflection function of the target in the frequency domain. Equation (3) also defines the "transducer response function", Φ, a frequency dependent quantity which will not change if the input signal to the transducer and range of the scatterer are kept the same. The most general theoretical expression for scattering from homogeneous, elastic spheres is given by Faran [3] in terms of a non-dimensional quantity called the "form function" $f(\omega, \theta, \phi)$,

$$|f(\omega, \theta, \phi)| = \lim_{r \to \infty} \frac{2r}{a} \left| \frac{p_s(\omega)}{p_i(\omega)} \right|, \tag{4}$$

where ω is the angular frequency, θ, ϕ scattering direction angles and a is the radius of the sphere. The condition on r implies that p_s is in the far field of the sphere. From equation (1) and (4) it follows that

$$\sigma_{bs} = \frac{a^2}{4} \left| f(\omega, -\pi, 0) \right|^2. \tag{5}$$

Assume now that $V_{m,s}$ is measured from a sphere of known form function, $|f_s|$, and $V_{m,o}$ from a different object, located at the same position. Equation (1) applies to both targets, and since I_i is the same for both,

$$\sigma_{bs,o} = \sigma_{bs,s} \frac{|I_{bs,o}|}{|I_{bs,s}|} = \frac{a^2}{4} |f_s|^2 \left(\frac{|V_{m,o}|}{|V_{m,s}|} \right)^2, \tag{6}$$

where $\sigma_{bs,s}$ is substituted from equation (5). Thus, the target strength of the object, according to equation (2), is

$$TS_{bs,o} = 20 \log_{10} \left(\frac{a}{2r_0} |f_s| \frac{|V_{m,o}|}{|V_{m,s}|} \right). \tag{7}$$

There is a close relation between $|f|$ and $|\hat{\mathcal{R}}|$,

$$|\hat{\mathcal{R}}| = \frac{a}{2r_0} |f_s|, \tag{8}$$

obtained from equation (4) by inserting for p_s. Substituting $|\hat{\mathcal{R}}|$ given in equation (8) in the right side of equation (3), an alternative expression for Φ is found,

$$\Phi = \frac{2r_0}{a} \frac{|V_{m,s}|}{|f_s|}. \tag{9}$$

The target strength of the object is therefore

$$TS_{bs,o} = 20 \log_{10} \left(\frac{|V_{m,o}|}{\Phi} \right). \tag{10}$$

Document downloaded by @DAEL, 2026-11-15 00:34:39 - personal use only

If the unknown scatterer is also a sphere this may now be applied to calculate the "measured form function" of this target,

$$|f_o| = \frac{2r_0}{a}\frac{|V_{m,o}|}{\Phi}, \tag{11}$$

where a now is the radius of the target. Most electroacoustical transducers are reciprocal which implies that $|g_1| = |g_2| = |g|$, and accordingly

$$|g|^2 = \left(\frac{r}{r_0}\right)^2 \frac{\Phi}{|V_t|}. \tag{12}$$

If the signals are measured at the input of the transmit amplifier and the output of the receiving amplifier the transducer transfer functions should be multiplied with those of the amplifiers. Thus, $g_1 \rightarrow g_1 \cdot g_p$ and $g_2 \rightarrow g_2 \cdot g_r$, where g_p is the transfer function of the power amplifier and g_r that of the receiving amplifier. Φ now represents the "system response function" rather than the "transducer response function", and reciprocity can no longer be assumed. Still, if the frequency response of the amplifiers are constant over the relevant frequency range, equation (12) may be used to calculate the frequency response of the transducer transfer function, apart from a constant amplitude coefficient.

3. Experiment

3.1. Set up

The measurements were made in a laboratory tank of dimensions $4 \times 1 \times 1\ m^3$ filled with tap water at room temperature about 21^oC. The tank was filled at least 14 days before measurements to ensure temperature stability and that dissolved air had disappeared to prevent air bubbles to form on the target or the transducer. Four different Simrad split-beam transducers were used: ES120-7CD with nominal resonance frequency 120 kHz, ES200-7CD with nominal resonance 200 kHz, and for some early measurements ES70-7C with nominal resonance 70 kHz and ES400-7C - a 400 kHz prototype transducer. All transducers had beam widths (-3 dB) close to 7 degrees. The split beam facility was not used. The transducers were mounted centrally at mid water depth at the end of the tank and aligned with horizontal sound axis. ES120-7CD and ES200-7CD were mounted at opposite ends of the tank and could be used at the same target without realignment.

Figure 1 shows a sketch of the instrumentation. The sphere targets were suspended from a rotary table mounted on a trolley rolling on rails along the longest side of the tank. A positioning device allowed careful alignment of the sphere to the sound axis using an under-water camera and a reference background screen fixed to the trolley. Both were removed during the acoustic measurements. The accuracy of the positioning is better than ±1 mm vertically and horizontally. A list of the spheres and their suspensions is given in Table I. The uncertainties in density

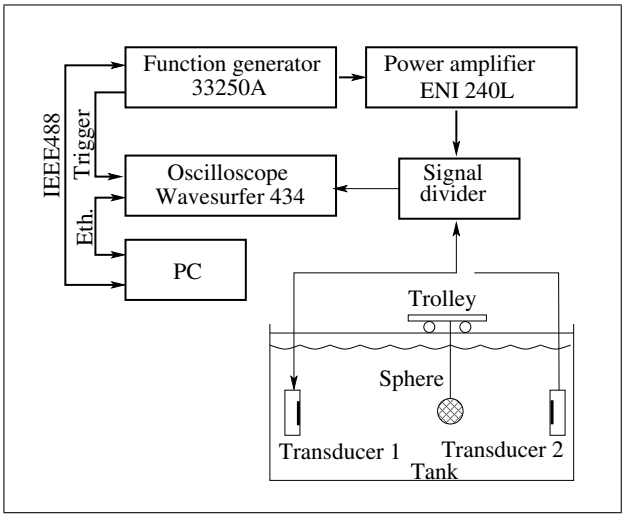


Figure 1. Instrumentation lay-out.

Table I. List of spheres. N=net, B=bare, L=loop.

Id.	Diam. [mm]	Weight [g]	Density [kg/m^3]	Gut dia. [mm]	Susp.
WC22	21.96	82.58	14812±2	0.32	N
WC38.1	38.10	432.28	14928±0.4	-	B
WC75	75.00	3294	14912±4	0.8	N
WC84	84.00	4630	14919±3	0.8	N
Cu30-A	30.02	126	8842±70	0.32	L
Cu30-B	30.00	125	8842±70	0.81	L
Cu30-C	30.00	125	8842±70	0.64	L
Cu30-D	30.00	125	8842±70	0.37/0.64	2L
Cu30-E	30.00	125	8842±70	0.64	L
Cu30-F	30.00	125	8842±70	0.64	L
Cu60-Old	59.92	1010	8966±9	-	B
Cu60-New	59.96	1010	8948±9	-	B

is largely due to a ±1 g uncertainty in the weight (except WC22 and WC38.1 where it is ±0.01g). The actual value of density has very little influence on the form function. In the simulations it is put to 14888 kg/m^3 for the WC-spheres and 8983 kg/m^3 for the Cu-spheres.

The signal generator was an Agilent 33250A Function/Arbitrary waveform generator programmed for most measurements to generate linear chirps of constant amplitude and 600 μs length. For the 120 kHz transducer the chirp covered $80 - 160$ kHz, and for the 200 kHz: $160 - 300$ kHz. The chirps, smoothed slightly with a Hanning window, were generated by Matlab code and uploaded to the function generator. Figure 2 shows the 200 kHz chirp and its spectrum as measured at the power amplifier input. The two large WC spheres, WC75 and WC84, were measured with single frequency bursts of about the same length and frequency steps of 100 Hz in the range 60–128 kHz.

The transmit signals were amplified with an ENI 240L power amplifier covering the frequency band 20 kHz - 10 MHz. A signal divider based on diode circuitry was used to avoid saturation of the oscilloscope by the trans-

Document downloaded by @DAEL, 2026-11-15 00:34:39 - personal use only

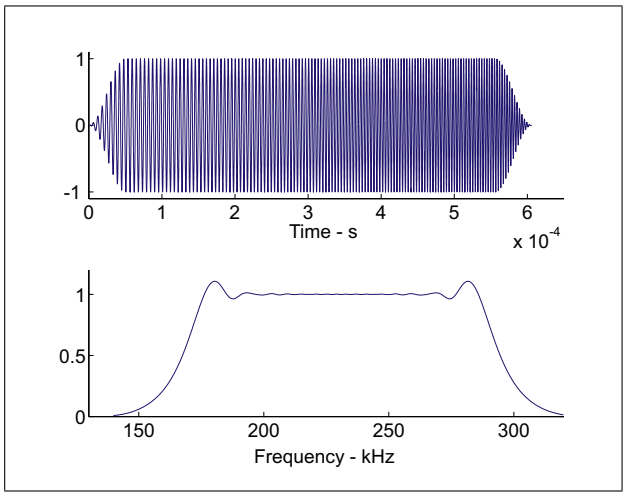


Figure 2. 200 kHz chirp and its frequency spectrum.

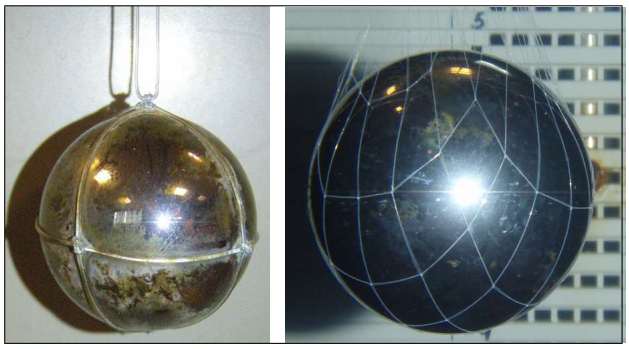


Figure 3. Left: Sphere WC22 in nylon netting. Right: Sphere WC38.1 in hair net.

mitted signal. The signal was recorded with a LeCroy Wavesurfer 434 oscilloscope with a sampling clock of 10 ns intervals (except for WC75 and WC84 where the oscilloscope was a Tektronix TDS220). All echoes were averaged in the oscilloscope over 25 bursts and downloaded to a PC for store and analysis.

To ensure proper warm up of the instruments they were kept running for several hours before measurements were recorded.

3.2. Procedure

3.2.1. Suspension methods

The suspension of the spheres is a special issue. As seen in Table I the spheres were equipped with three different suspensions. WC22, WC75 and WC84 were embedded in a coarse netting knit of monofilament nylon gut (fishing line). The netting was made of two orthogonal meridian circles and one equatorial circle, with knots at the crossings and a loop attached at one pole - see Figure 3, left. It was knit from a single tightly wound filament. The WC38.1 and the two Cu60 spheres were bare, and were suspended in a finer net of monofilament (two strands) gut of diameter 0.04 mm, e.g. a type of "hair net". The suspensions of the WC22 and WC38.1 spheres are shown in Figure 3.

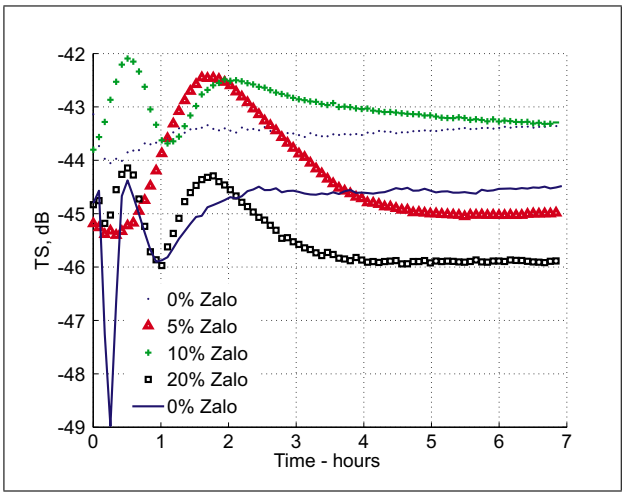


Figure 4. Echo amplitude of WC22 dipped in detergent solution as a function of time after suspension in water. 400 kHz.

All of the copper spheres of diameter 30 mm were provided with a monofilament loop of nylon gut fixed in a hole drilled into the sphere (one with two loops attached at opposite poles). Except for WC75 and WC84 the sphere suspensions were further attached with a nylon gut of diameter 0.18 mm to the positioning device.

A separate study of the WC38.1 sphere suspended in a nylon netting (like Figure 2, left) and rotated 350 degrees showed variations of about 0.85 dB at 120 and 150 kHz. When it was suspended in a hair net the amplitude variations were less that 0.1 dB when rotated.

Traditionally it has been recommended that the spheres and suspension should be moisted in a solution of detergent and water before immersed into water, in order to get rid of the air. To investigate the influence of wetting agent on the nylon gut a special series of measurements were made. The WC22 sphere was dipped in different solutions of water and detergent (Zalo), rubbed with fingers for some seconds while embedded in the solution, and then suspended in the tank (with a brief exposure to air). After careful alignment to the sound axis measurements started about 15 minutes after the sphere was moved to the tank. Echoes were recorded every 5 minutes for 17 hours or longer. The transducer used was the Simrad ES400-7C. The solutions had concentrations 0, 5, 10 or 20 % detergent in water. Records were taken at frequencies 300–500 kHz in steps of 1 kHz. The results show in general large variations in amplitude lasting for at least 5 hours, regardless of the Zalo concentration. A typical example is presented in Figure 4, which shows the echo amplitude versus time at 400 kHz.

In our set up the side of the sphere is facing the transducer, and the echo will depend on the actual rotation angle. In Figure 4 the final values after 7 hours differ, which is believed to be caused by different orientation of the sphere and netting. A separate measurement confirms this. Figure 5 shows the frequency dependent TS of two cases, 10% and 20% solution after 7 hours. After such a long time all air is supposed to be dissolved. Thus, the differ-

Document downloaded by @DAEL, 2026-11-15 00:34:39 - personal use only

ence between the two curves must be due to the combined effect of the netting and using detergent of different concentrations. The WC22 sphere was left in the tank over a week-end, and then measured. Subsequently it was rotated 2 degrees, and again measured. The difference in amplitude was 0.8 dB at 400 kHz, and could only be due to the change of orientation of the netting.

Our conclusion from this experiment is that it takes at least 5 hours for the echo to stabilize regardless if it has been dipped in detergent or not, at least at such shallow depths (0.5 m). For this reason the spheres and suspensions were hung in water at least one day before alignment. This was also necessary in order to let the suspension stabilize lengthwise (between the measurements shown in Figure 4 the spheres hung in the suspension in air to keep the gut stretched). Moreover, the influence of the netting has been shown to be non-negligible, and other ways to suspend the spheres should be encouraged.

3.3. Inversion of sphere parameters

In order to be able to utilize spheres for calibration purposes it is essential to know as accurately as possible the parameters governing the form function. The following sphere parameters are relevant, assuming that the sphere is homogeneous and the sphericity is close to one: density: ρ_{sph}, radius: a, compressional wave speed: c_L and shear wave speed: c_S. In addition two parameters associated with the medium: density: ρ_W and sound speed: c_W. The medium parameters ($\rho_W = 1000$ kg/m^3, $c_W = 1490$ m/s), the sphere density and radius are easily determined, so the emphasis here is on the two wave speeds in the sphere.

Our starting point is the spectrum of the measured echo from the sphere. The most significant features are the deep dips (nulls) in the spectrum. The location of the major dips in the form function are very sensitive to the wave speeds in the sphere, in particular to the shear wave speed. Figure 6 shows an example of the measured echo, the spectrum of this echo and the corresponding simulated form function for the WC38.1 sphere with the 200 kHz chirp. The form functions were computed based on Faran's solution [3].

The task is to find matching pairs of c_L and c_S, trying to fit the theoretical form function to the measured spectrum. Different approaches were tried. A map of dip frequency locations [13] as function of both wavespeeds is useful for identifying which dips are most sensitive to wavespeed changes. However, a better procedure is to use a Nelder-Mead Simplex minimization algorithm [14]. The challenge is to find a good cost function, measuring the difference between the simulated form function and the measured spectrum. The simplex algorithm minimizes the cost function by adjusting c_L and c_S. A good candidate cost function is the root-mean-square difference between simulated and measured dip frequencies: $c = \sqrt{\sum_j (f_{s,j} - f_{m,j})^2}$, where $f_{s,j}$ is the frequency of dip j in the form function, and $f_{m,j}$ in the measured spectrum.

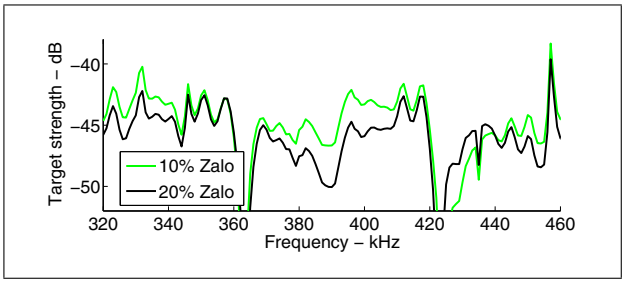


Figure 5. TS of WC22 after 7 hours, dipped in detergent of 10% and 20% solution.

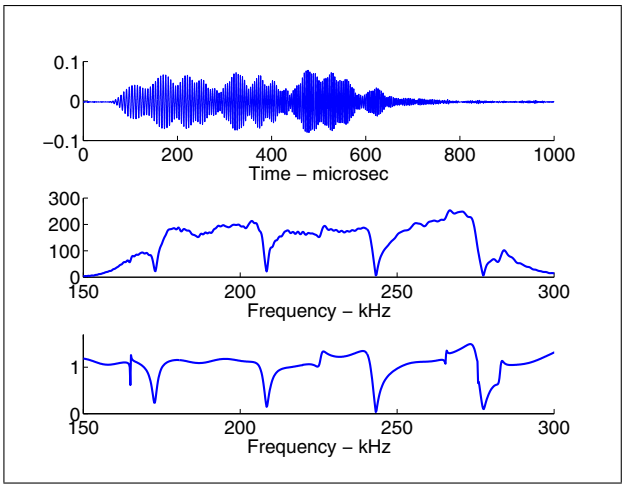


Figure 6. WC38.1 with 200 kHz chirp. Top: received echo, Middle: spectrum of echo, Bottom: corresponding theoretical form function.

The measured sphere spectra, with frequency resolution 100 Hz, were obtained by appending sufficient number of zeroes to make the signal length 10 ms before taking the Fourier transform. Subsequently they are analysed by an algorithm which locates the deep minima. The frequencies of representative dips are selected to be used in the inversion process. Based on chosen start conditions for the sound speeds, together with the other sphere- and medium parameters, the form function is computed (not including absorption) and the simulated dips located and the relevant ones selected according to certain criteria. The cost function is now computed, and is then input to the simplex routine which returns an improved set of wave speeds. The new form function is computed, the dips located, the cost function computed, and the process repeated for 50 iterations. Figure 7 illustrates a typical search in the simplex process, showing the successive choices of the two wave speeds, optimizing for the WC22 sphere. The uncertainty of the resulting wave speeds is found as the standard deviation of values found with the final cost function below a certain threshold, using different starting conditions in the simplex algorithm.

A problem is that as the wave speeds are changed some simulated dips may disappear while others appear, and in an automated process it is easy to choose wrong dips for comparison. Thus, it is necessary to adjust from case to

Document downloaded by @DAEL, 2026-11-15 00:34:39 - personal use only

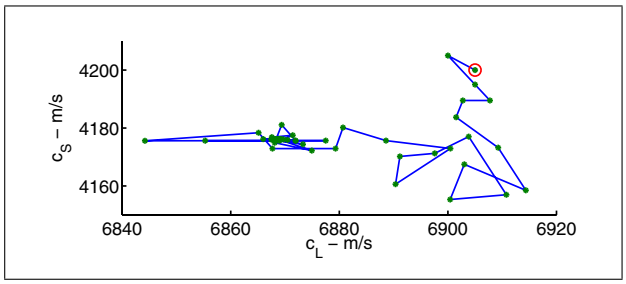


Figure 7. Typical simplex iteration map for the WC22 sphere. The circled point indicates start of search.

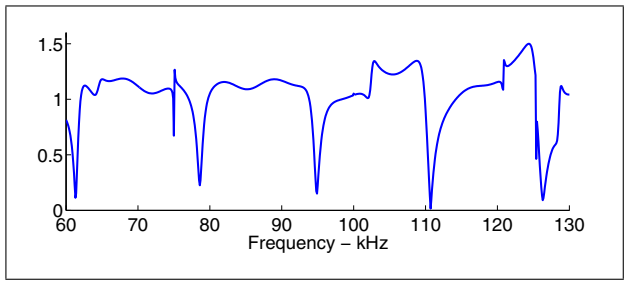


Figure 8. WC84 form function computed with wave speeds optimized for WC84.

Table II. Frequency of dips for WC-spheres - kHz.

WC22, Dips used:			157.8	200.6	234.2	
120 kHz:			157.6			
200 kHz:			157.8	200.6	234.2	299.8
Form function			157.8	200.6	234.2	300.0
WC38.1, Dips used:			172.9	208.4	243.2	275.5
120 kHz:	90.9	135.0				
200 kHz:			172.9	208.4	243.2	275.5
Form function:	90.7	134.8	172.7	208.5	243.3	277.7
WC75, Dips used:	68.5	88.1	106.3	124.1		114.8
Form function:	68.7	88.1	106.3	124.1		114.8
WC84, Dips used:	61.1	78.5	94.9	110.7		102.4
Form function:	61.3	78.6	94.9	110.7		102.4

Table III. Optimized wave speeds for the WC spheres - m/s

ID:	c_L	c_S
WC22	6867 ± 2	4176.2 ± 0.4
WC38.1	6873 ± 9	4159 ± 3
WC75	6884 ± 6	4178 ± 2
WC84	6880 ± 4	4175 ± 2

case the criteria used in selecting the wanted dips. Moreover, the simplex algorithm does not guarantee that the best inversion is found. There may be several local minima in the cost function which traps the algorithm, so several runs with varying starting conditions are necessary. In addition, it sometimes happens that different runs end up with the same dip-frequencies for unequal sets of wavespeeds. In such cases additional features of the form function are needed in the search, like location of smaller dips or step-like changes in amplitude.

3.4. Results

3.4.1. WC spheres

The dips located in the measured spectra of the WC spheres which were used for inversion are presented in Table II. For WC22 and WC38.1 are also shown the other dips found with 120 and 200 kHz chirps, and finally the dips resulting from the optimized form functions. The locations of the measured dips for these two spheres were better than ± 100 Hz, based on repeated measurements. The simplex inversion process uses start conditions with $6800 < c_L < 6900$ m/s and $4100 < c_s < 4200$ m/s. For the WC22 sphere the inversion gave a complete match (zero cost function) and very little spread in final wave speed values. As seen in Table II also the dips not used in the inversion fits within 200 Hz of the form function values. The WC38.1 sphere has a larger uncertainty due to a multitude of local minima in the inversion process.

The WC75 and WC84 spheres required more attention. Using only the big dips, c_L is not located better than ± 70 m/s, and it is necessary to look for other features to narrow down this wave speed. It turns out that the form function of both spheres shows one or two step-like discontinuities, like the one seen in Figure 8 near 103 kHz, which are sensitive to c_L in particular. The measurements were only made with the 70 kHz transducer for these spheres. Table II shows the measured dips used for the WC75 and WC84 spheres, and those found with the optimized wave speeds. The frequency in the last column represents the central point in the step-like discontinuity.

Table III shows the optimized wave speeds for the WC spheres.

3.4.2. Copper spheres

Copper spheres were originally chosen for calibration purposes because copper is easily available in a very pure state. Even if copper is known not to be allotropic it may be subject to hardening by cold working which decreases the malleability [15]. This is often encountered in water copper pipes some time after plumbing and may possibly cause a change in the elasticity modules. For the purpose of investigating any variation between different copper spheres, IMR provided us with a selection of 9 different spheres. Seven of these spheres are of diameter 30 mm, of unknown age (typically 20–30 years), 2 of diameter 60 mm – one old (30 years) and one newly made.

The same procedure as for the WC38.1 and WC22 spheres was used with the copper spheres.

Figure 9 shows a typical form function for copper spheres with frequency axis in dimensionless form (ka, k is wavenumber) for greater universality. The individual dips are identified by letters for reference.

3.4.3. 30 mm spheres

Some of the dips shown in Figure 9 are less useful for automatic search for parameter fitting because of great variability in amplitude or closeness to neighbouring dips. In particular this goes for dips marked A_1, D_1, F and H_1.

Document downloaded by @DAEL, 2026-11-15 00:34:39 - personal use only

Table IV. Frequency of dips used with the Cu30 spheres - kHz.

Sphere id	C	D	E	G	H	I
Cu30-A	125.0	152.3	180.1	234.5	259.4	284.2
Cu30-B	125.0	152.6	180.6	234.1	260.4	285.0
Cu30-C	124.9	152.1	180.3	234.3	259.0	286.0
Cu30-D	125.0	152.0	179.2	234.5	259.4	284.6
Cu30-E	124.8	152.1	180.0	234.5	258.9	285.4
Cu30-F	124.9	152.7	179.3	234.4	259.3	284.7
Cu30-G	125.0	152.0	180.5	234.4	259.4	284.9
Average:	124.9	152.3	180.0	234.4	259.4	285.0
Std. dev.	0.1	0.3	0.6	0.1	0.5	0.5

Table V. Wave speeds for Cu30 spheres - m/s.

Sphere id	c_L	c_S
Cu30-A	4779.5	2242.5
Cu30-B	4775.5	2247.5
Cu30-C	4778.5	2246.5
Cu30-D	4778.7	2242.5
Cu30-E	4782.0	2244.0
Cu30-F	4781.0	2244.0
Cu30-G	4781.5	2244.0
Average:	4780±11	2244.4±2

For the Cu30 series of spheres good results were obtained with dips C, D, E, G, H and I. Despite the various (partly unknown) ages and different size of suspension guts, no significant variation in dip frequencies was detected, as shown in Table IV. Nor was any significant variation in wave speeds found when inverting the individual spheres - see Table V. The averaged speeds estimated from inversion are $c_L = 4780 \pm 11$ m/s and $c_S = 2244 \pm 2$ m/s. Taking the average of the dip frequencies as input to the simplex algorithm results in almost the same values: $c_L = 4783 \pm 8$ m/s and $c_S = 2244 \pm 1$ m/s. The accuracy is estimated as described above.

Table V shows the results for all Cu30 spheres. The final cost function has a mean value of 1.0 kHz, averaged over all spheres.

Figure 10 shows the measured and simulated form function ($c_L = 4780$ m/s and $c_S = 2244$ m/s) for Cu-30A as a typical example. The range 100–160 kHz was measured with the 120 kHz transducer while the 160–300 kHz was measured with the 200 kHz transducer. The measured form function was obtained using equation (11) and response function Φ as shown in section 2.

3.4.4. 60 mm spheres

One of the two spheres is probably about 30 years old while the other is quite recently manufactured. Both were without suspensions attached and accordingly were hung in a hair net like the one used for WC38.1. The same measurements as for the Cu30 spheres were taken, and in addition the spheres were rotated 360 degrees in steps of 10 degrees. If any change in wave speeds would occur due to ageing this should be clearly evident in these spheres. Because of the large size of these spheres the form function looks rather complicated with the 200 kHz chirps, so the 120 kHz chirp results are shown here.

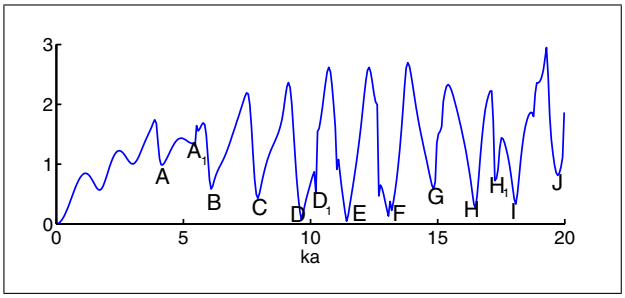


Figure 9. Copper sphere form function.

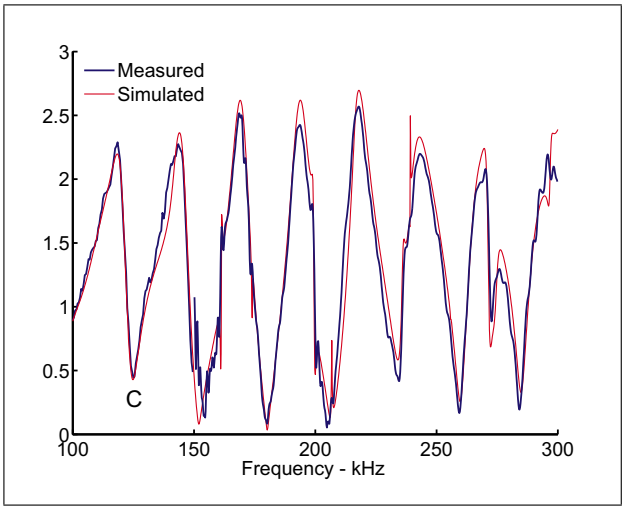


Figure 10. Measured and simulated copper sphere form function for Cu30-A. The first dip corresponds to dip C in Figure 9.

Table VI. Dip frequencies and wave speeds for Cu60 spheres.

Cu60-old					
Dips used	90.8	118.3	131.1	144.0	(156.6)
Form function	90.8	118.3	131.1	143.9	(156.9)
Optimal c_L	4775±11 m/s				
Optimal c_S	2270.0±0.2 m/s				
Cu60-new					
Dips used	90.8	118.2	131.1	144.1	(157.6)
Form function	90.8	118.3	131.1	143.9	(156.9)
Optimal c_L	4775 ±11 m/s				
Optimal c_S	2270.0±0.2 m/s				

Table VI summarizes the mean values of dip frequencies used for inversion. Figure 11 shows typical measured form functions for the two spheres and simulations based on the best fitted wave speeds.

For Cu60-New the inversion at each angle of rotation results in the averaged values $c_L = 4734.7 \pm 0.5$ and $c_S = 2275.6 \pm 0.9$ m/s, while using the average of the dip frequencies results in $c_L = 4775 \pm 11$ and $c_S =$

Document downloaded by @DAEL, 2026-11-15 00:34:39 - personal use only

2270.0±0.2 m/s with a final cost function equal to 150 Hz. The latter values are used in the simulations in Figure 11.

For Cu60-Old the same procedure results in $c_L = 4734.8 \pm 0.5$ and $c_S = 2275.5 \pm 0.8$ for the averaged values found at each angle, and the same values as for Cu60-New using the average of the dip frequencies. The difference seen in these values of c_L reflects the relative insensitivity of the dip frequencies to the actual value of c_L, and the weakness of the simplex algorithm. For each rotation angle the same starting conditions in the search were used, and only results with the cost function below a certain threshold (0.3 kHz) were accepted. Inversion on the mean of the dip frequencies was made with many different starting conditions, since only one set of dips needed to be inverted. Thus, these values are considered to be more reliable. In practice, the difference between form functions using $c_L = 4735$ and $c_L = 4775$ is marginal for most of the frequencies.

The results strongly suggest that there be no significant difference between the parameters of these two spheres, thus asserting that ageing has negligible effect on the acoustic scattering properties of copper spheres.

In neither of the two spheres could systematic variations in the dip frequencies or the inverted wave speeds with rotation angle be detected. This indicates that the spheres are homogeneous and isotropic in their acoustic scattering properties.

4. Broad band calibration

4.1. Simrad ES200-7CD 200 kHz transducer

Figure 6 shows the received signal with the WC38.1 sphere centred in the beam at about 2.5 m range. It also shows a plot of the amplitude spectrum of this signal. Lastly, this figure shows the computed form function for the WC38.1 sphere, with wave speeds adjusted to match the dips in the spectrum ($c_L = 6873$ m/s and $c_s = 4159$ m/s).

Equation (9) now allows calculation of the response function Φ for this transducer and range, as shown in Figure 12. Here is also shown the result when Φ is filtered to remove the big spikes and the small noisy fluctuations. It is necessary to have optimized wave speed values for the sphere in order to reduce the amplitude of these spikes. Even if the dips in the spectrum and the form function match they do not cancel completely.

Various options may be used to reduce the spikes resulting from this. A first attempt was to substitute the area near the spikes by manually drawing a sloping line across these areas. A better approach was to reduce the spikes in the raw version of Φ by substituting average values in such regions, followed by a "low frequency" filter. This is a rectangular window applied to the FFT of the response function, followed by an inverse transform. An example of this is shown in Figure 12. Figure 13 shows similar results for the WC22 sphere.

Since the spikes in the Φs for WC22 and WC38.1 appear at different frequencies it would be tempting to use different parts of the two response functions to eliminate these fluctuations [10, 11]. However, the absolute values of the two Φs differ too much to make this a reliable method. Filtered versions of these two response functions eliminate the worst fluctuations, as shown in Figure 14, but they are still different.

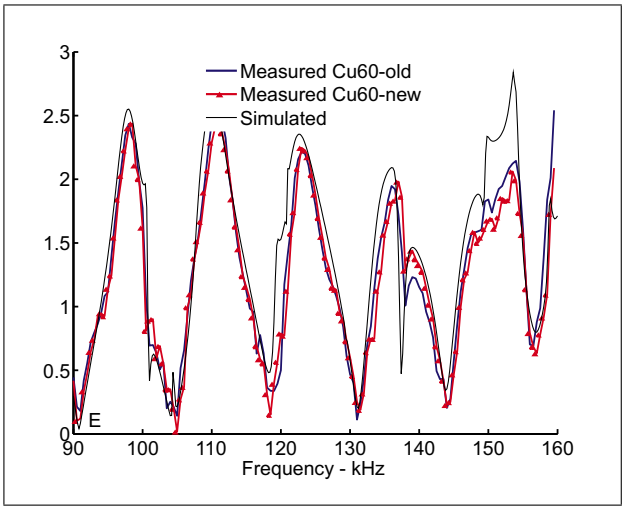


Figure 11. Measured and simulated copper sphere form function for Cu60 old and new. The first dip corresponds to dip E in Figure 9.

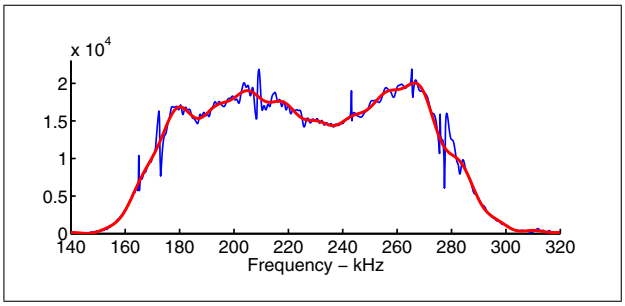


Figure 12. Calculated transducer response Φ WC38.1, raw and filtered, 200 kHz chirp.

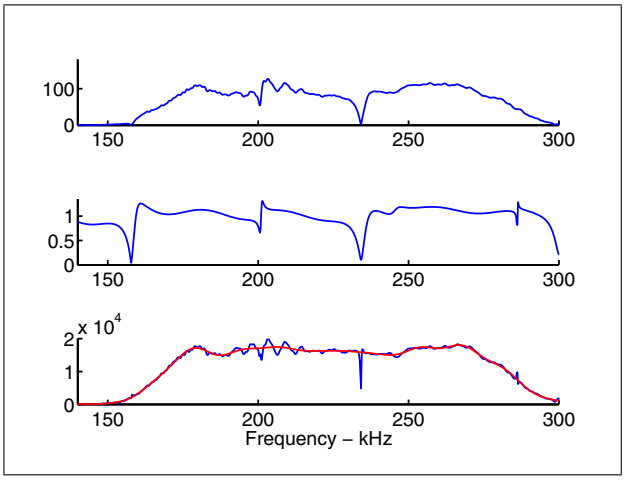


Figure 13. WC22 with 200 kHz chirp. Top: spectrum, Middle: form function, Bottom: raw and filtered version of Φ.

Document downloaded by @DAEL, 2026-11-15 00:34:39 - personal use only

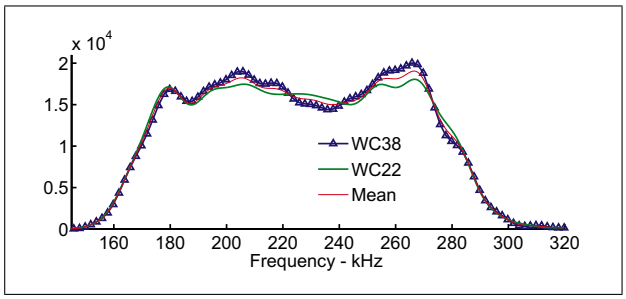


Figure 14. Filtered Φ from both spheres, and their average. 200 kHz chirp.

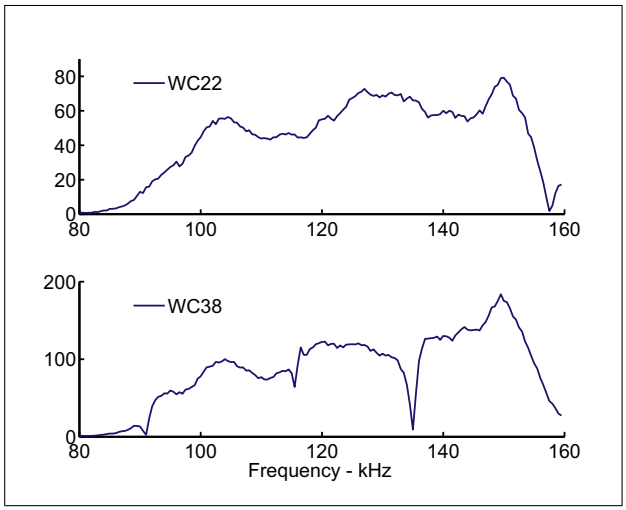


Figure 15. Amplitude spectra of WC22 and WC38.1 with a 120 kHz chirp.

This difference may originate in the suspension of the WC22 sphere. The WC38.1 sphere is hanging in a much finer net and is not supposed to be subject to such variation. Therefore a greater confidence ought to be put on Φ measured with this sphere. Still, in this example the mean of the two was taken, while the difference was used to get an estimate of the uncertainty of the measurements.

4.2. Simrad ES120-7CD 120 kHz transducer

The same WC spheres and the same procedure as above is used at a range of 2.1 m. The corresponding spectra are shown in Figure 15. In this case the response functions determined by the two spheres are much more alike than for the 200 kHz case as is demonstrated in Figure 16.

It is not necessary to remove spikes, just to filter. Figure 17 shows the filtered Φs and their average.

The target strength of the spheres, calculated from equation (10) is shown in figures 18–19, composed from both chirps. Below 155 kHz the response function for 120 kHz chirp is used, above 155 kHz the one for 200 kHz. The figures show the mean measured TS (using the averaged Φ), with errorbars based on the two individual Φs, and the simulated TS based on the form function.

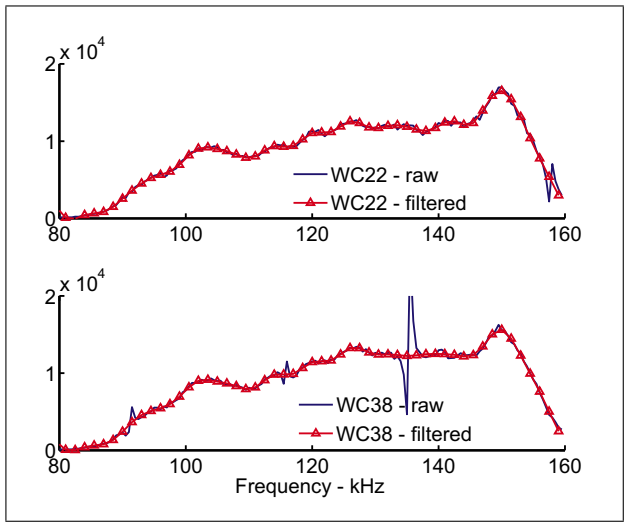


Figure 16. Φ, WC22 and WC38.1, raw and filtered with 120 kHz chirp.

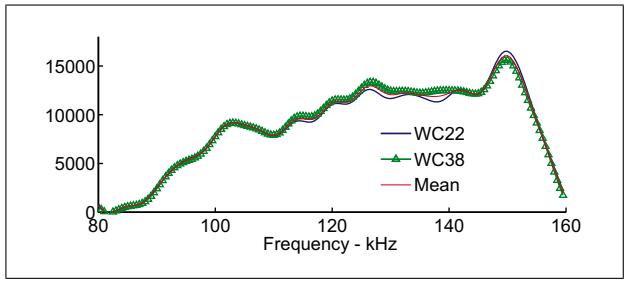


Figure 17. Φ, WC22 and WC38.1, filtered and averaged, 120kHz chirp.

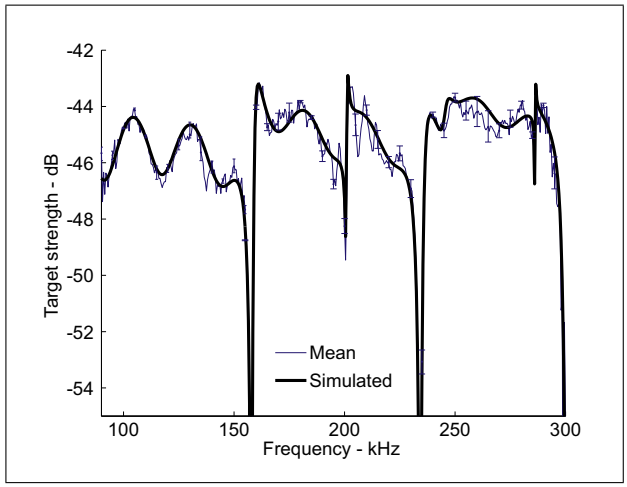


Figure 18. WC22, measured and simulated TS.

4.3. Transducer frequency response

The amplitude of the transducer transfer function may be calculated from equation (12) assuming reciprocity. In our case the forward transfer function also contains that of the power amplifier and the receiver amplifier. These are assumed to be flat in the region 20 kHz - 10 MHz, so in the result they appear as a constant factor. Figure 20 shows the result for the ES120-7CD and ES200-CD transducer, tak-

Document downloaded by @DAEL, 2026-11-15 00:34:39 - personal use only

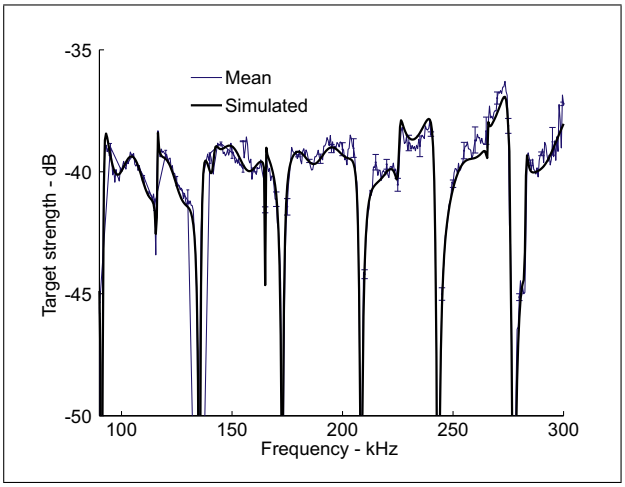


Figure 19. WC38.1 measured and simulated TS.

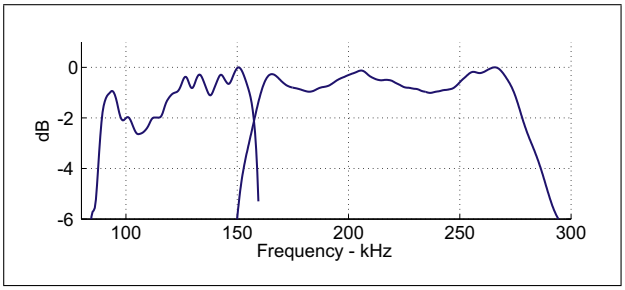


Figure 20. Transducer frequency response for ES120-7CD and ES200-7CD.

ing the square root of the ratio of Φ (averaged for WC38.1 and WC22) and the spectrum of the chirp. The plot is in dB after normalisation with the maximum value. In this way the amplifier constant is eliminated. The -3dB bandwidth is seen from this figure to be 88 - 158 kHz for ES120-CD and 156 - 281 kHz for ES 200-CD.

The assumption of reciprocity is not unreasonable, but has not been tested for these particular transducers. Anyway, this method seems to give acceptable results for the transducers at hand, and is a quick way to measure the transducer frequency response without requiring more sophisticated equipment. Of course, in order to obtain absolute amplitude calibration a more careful approach is necessary, for example using measurements of the current in the transmitter.

5. Discussion and summary

5.1. Suspension

It is shown that the way a sphere is suspended may have some influence on the target strength. This is especially evident if the sphere is tiny and the nylon gut is knit like a netting about the sphere. The reason is twofold: reflections from the nylon gut itself and the presence of tiny micro-bubbles of air inside the knots. When the sphere is sonified from a side, the rotation angle of the sphere has an influence. When the sphere is sonified from above or from below, as in common echo sounder calibration, the rotation angle is irrelevant, but the netting still may modify the target strength. In our experience it takes at least 5 hours before the echoes are stable, regardless if the sphere is soaked in detergent or not. Whether this is due to dissolving of micro-bubbles or water penetration into the nylon gut is not known. It is possible that this process is faster at greater depths than used here (0.5 m).

When the spheres were suspended in a nylon hair net of gut diameter 0.04 mm no effect of the suspension was observed. Also here the sphere and net was soaked for at least 5 hours. The Cu30 spheres were suspended in loops of nylon line attached in a hole drilled into the sphere (without a netting). Here no effect of the suspension was detected (except possibly from the hole itself).

5.2. WC spheres

The WC spheres show a great similarity in c_S, except for WC38.1 which lies about 20 m/s lower than the rest. The c_L values lie fairly close to each other. For WC75 and WC84 c_L had to be determined using a step-like discontinuity in the spectrum in addition to the big dips. This discontinuity shows little sensitivity to choices of c_S, and it is possible to find an approximately linear relation between its frequency and c_L. Thus, we are confident that the quoted values are correct. To compare with previous values reported in the literature: Neubauer *et al.* [5]: $c_L = 6860$, $c_S = 4185$ m/s, Gerlich *et al.* [16]: $c_L = 6864 \pm 69$, $c_S = 4161 \pm 21$ m/s, MacLennan *et al.*[6]: $c_L = 6853 \pm 19$, $c_S = 4171 \pm 7$ m/s. The present values differ not much from these.

The WC spheres were supplied from the same manufacturer, Spheric-Trafalgar LTD, London, UK, but at different times (WC75 and WC84 were delivered simultaneously). Nominally they are of equal composition (6% cobalt binder), but admittedly it is very hard to make alloys exactly similar in different batches, like spatial uniformity and distribution of the components. It has recently been questioned whether exposure to water may change the elastic properties of tungsten carbide due to penetration of water [17], but it is hard to believe that a molecular thick layer on the sphere surface can have high enough influence to be of significant importance. The influence of changes in the sphere density and water sound speed on the form function is very small. For example, a change in c_W from 1486 m/s to 1500 m/s (equivalent to a temperature change from 21 to 26°C) shifts the mean of the absolute difference between the target strengths in the frequency range 140–320 kHz by 0.2 dB, and an increase of ρ_{sphere} by 5 % the same by 0.09 dB for the WC22 sphere. The shifts in dip frequencies are almost undetectable.

For a long time it has been known [5] that the shear wave speed is the parameter that has the largest influence on the locations of the dips in the form function. It should be pointed out that the exact location of the dips have little influence on the form function outside the dips. As an example, computing the form function of WC84 using the optimized values and those given by MacLennan *et al.*

Document downloaded by @DAEL, 2026-11-15 00:34:39 - personal use only

[6], the mean of absolute values of ΔTS over the whole frequency range is 0.48 dB, while for ranges between the dips it is 0.05 dB or less (ranges 66-74, 81-93 and 113-120 kHz). However, the maximum difference in TS (ΔTS) is 19.5 dB due to non-overlapping dips.

The same exercise on WC22 gives a maximum difference in TS of 8.5 dB in the frequency range 140–350 kHz, and the mean of absolute values of ΔTS 0.21 dB. For ranges between the dips it is 0.03 dB or less.

5.3. Copper spheres

The Cu30 spheres, of different ages and suspension details, are remarkably equal. The mean of the wave speeds determined individually are $c_L = 4780 \pm 11$ and $c_S = 2244 \pm 2$ m/s. Using instead the mean of the dip frequencies as input to the inversion we find $c_L = 4786 \pm 8$ and $c_S = 2244 \pm 2$ m/s. Foote [18] found $c_L = 4760$ and $c_S = 2288.5$ m/s.

The Cu60 spheres are also remarkably equal, considering the about 30 years difference in age. This implies that any ageing effects of copper does not influence acoustic scattering properties of the spheres. A difference in wave speeds is found if each rotation angle is inverted individually and then averaged, compared to averaging the dip frequencies before inversion. It is likely that the last procedure is the most accurate since for practical purposes the number of different starting conditions then was larger. Thus, the best values are $c_L = 4775 \pm 11$ and $c_S = 2270.0 \pm 0.2$ m/s. Both spheres converge strongly to the same shear wave speed. The compressional wave speed is almost the same as in the Cu30 spheres while the shear wave speed is about 25 m/s higher. All the Cu30 spheres have a hole drilled in the place where the nylon loop was attached. The Cu60 spheres has no drilled holes. We can not rule out that the hole has an effect of reducing the equivalent shear wave speed, and we have no other explanation.

5.4. Broadband calibration

Even if the sphere parameters were carefully adjusted to fit the big dips in the form function, the response function still contains spikes due to slight mismatch in the shape of the dips. By using two separate calibration spheres it might be possible to substitute parts from one response function to the other, since these spikes seldom coincide in frequency. However, at least for the 200 kHz chirp response functions the discrepancy between the amplitudes of the two was too big, and would cause steps in the response function. Instead the mean of the two was used, after removing the largest spikes with averages and "low frequency" filtering. For the 120 kHz chirp the two response functions were very similar, and the substitution method mentioned above could have been used, but filtering and averaging gave a satisfactory result. To validate the found response functions they are used to find the measured form functions of the WC22 and WC38.1 spheres and compared to the simulated ones, as shown in Figures 18–19. Figure 21 shows the magnitude of the difference between

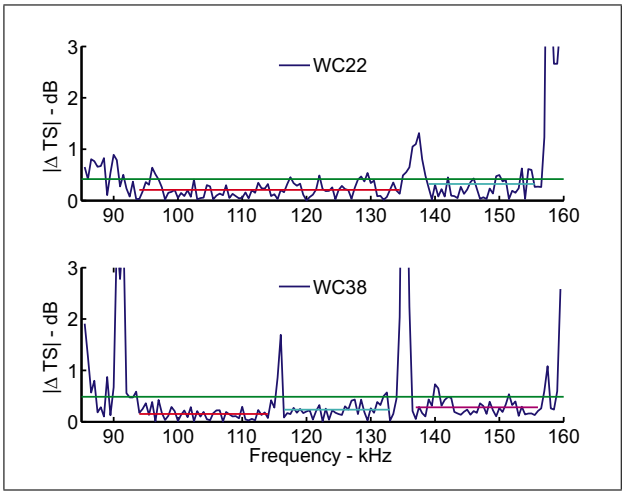


Figure 21. Magnitude of difference in measured and simulated TS for WC22 and WC38 with 120 kHz chirp. Horizontal lines indicate mean values in different regions.

measured and simulated target strength for both spheres with the 120 kHz chirp.

The mean value in the whole frequency range (88–158 kHz) is 0.42 dB for WC22 and 0.49 dB for WC38.1. Regions between the dips, as indicated by horizontal lines in the figure, have lower mean values, typically less than 0.3 dB for both spheres. For the 200 kHz chirp the mean difference between the measured and simulated form functions is 0.42 dB over the frequency range 160–300 kHz for both spheres. Also here the difference in the regions outside the dips is typically below 0.3 dB. A similar procedure applied to the WC84 sphere (calibrated using the WC38.1 sphere) gives similar results: 0.25 dB over the whole frequency range 58–130 kHz (including dips), and less or equal to 0.1 dB in bands between the dips. The largest deviations occur where there are dips in the target spectrum.

Thus, it is possible to obtain accuracy of about 0.3 dB or better over wide frequency ranges if the target has no such dips. The accuracy decreases near the outskirts of the response function.

5.5. Transducer frequency response

This method rests on reciprocity of the transducers, which has not been investigated for the transducers used here. Also, since the voltages are measured at the input to the power amplifier and at the output of the signal divider, the frequency response of these units are not included. However, there is reason to assume these to be constant over the frequency ranges in question, so they will have a negligible effect, and factor out when the result is expressed in dB normalized at the maximum value. Only the amplitude of the transducer frequency responses are obtained, and it is not possible to specify the accuracy without further knowledge of the transducer properties. For the transducers at hand the −3 dB bandwidths are 88–158 kHz for ES120-CD and 156–281 kHz for ES200-CD, respectively, so together they cover a band of 88–281 kHz.

Document downloaded by @DAEL, 2026-11-15 00:34:39 - personal use only

6. Conclusions

A netting of nylon monofilament gut wound tightly around the sphere may modify the target strength. Loops fixed to a tiny hole drilled in the sphere seems to be a better way of suspension. Another method is to use a bag of nylon hair net. Soaking in detergent has no effect on the time for micro-bubbles of air to become dissolved. The spheres should be kept in water for at least 5 hours before starting measurements.

For calibration purposes the wave speeds in the spheres should be known as precisely as possible. The big dips depend largely on the shear wave speed, and cause large peaks and dips in the response function Φ if misplaced in frequency. The shear wave speed can be found with good precision using the simplex method on several big dips. WC sphere wave speeds depend on the accuracy of the composition, in particular the amount of cobalt. Three of the spheres measured had c_S close to 4175 m/s while the fourth was about 15 m/s lower, most probably due to a variation in the composition.

The compressional wave speed has less influence on the dip locations, and is determined with lower accuracy by this method.

No ageing effects were detected in the copper spheres, nor any detectable variations due to the different suspensions, which were mostly loops of monofilament nylon of various diameters attached to a hole drilled in the sphere surface. There is a discrepancy of about 25 m/s between the shear wave speeds in the Cu30 spheres and the Cu60 copper spheres.

The response function is obtained from equation (9), followed by a filter to remove spikes due to slight displacement of the big dips in the spectrum with respect to the form function. It can be used in the frequency band covered by the transducer, provided the unknown target is positioned at the same range and position as the calibration sphere. Accuracy of about 0.4 dB has been obtained over this frequency band, and better for limited frequency ranges.

If the transducer fulfils reciprocity requirements ($|g_1| = |g_2|$) the amplitude of the transducer frequency response can be found by taking the square root of equation (12). This is a simple, although not exact way to find the frequency response.

Acknowledgement

We thank senior researcher Rolf J. Korneliussen and professor Egil Ona at IMR, Bergen, Norway for supplying calibration spheres and Simrad transducers, and for fruitful discussions. T.N. Forland wishes to acknowledge a PhD-fellowship from the Department of Physics and Technology, University of Bergen.

References

[1] K. Foote: Optimizing copper spheres for precision calibration of hydroacoustic equipment. J. Acoust. Soc. America **71** (1982) 742–747.

[2] D. MacLennan: The theory of solid spheres as sonar calibration targets. Scottish Fisheries Research Report No 22, 1981.

[3] J. J. Faran: Sound scattering by solid cylinders and spheres. J. Acoust. Soc. America **23** (1951) 405–418.

[4] R. Hackman: Acoustic scattering from elastic solids. – In: Physical Acoustics Vol XXII. Underwater Scattering and Radiation. A. Pierce, R. Thurston (eds.). Academic Press, 1993.

[5] W. G. Neubauer, R. H. Vogt, L. R. Dragonette: Acoustic reflection from elastic spheres. I. Steady state signals. J. Acoust. Soc. America **55** (1974) 1123–1129.

[6] D. MacLennan, J. Dunn: Estimation of sound velocities from resonance measurements on tungsten carbide calibration spheres. J. Sound Vib. **97** (1984) 321–331.

[7] L. R. Dragonette, S. K. Numrich, L. J. Frank: Calibration technique for acoustic scattering measurements. J. Acoust. Soc. America **69** (1981) 1186–1189.

[8] T. K. Stanton, D. Chu: Calibration of broadband active acoustic systems using a single standard spherical target. J. Acoust. Soc. America **124** (2008) 128–136.

[9] K. Foote, D. Francis, H. Furseth, H. Hobæk: Spheres for calibrating high-frequency broadband echo sounders. J. Acoust. Soc. America **105** (1999) 1112–1113.

[10] P. R. Atkins, D. Francis, K. G. Foote: Calibration of broadband sonar systems using multiple standard targets. Acoustics 08 Conference Proceedings, 2008, 2821–2826.

[11] E. Ona, L. N. Andersen, H. P. Knudsen, S. Berg: Calibrating multibeam, wideband sonar with reference targets. OCEANS 2007 - IEEE Conference proceedings, Aberdeen, 2007.

[12] A. Islas-Cital, P. R. Atkins, K. Y. Foo, R. Picó: Broadband amplitude and phase sonar calibration using lfm pulses for high-resolution study of hard and soft acoustic targets. OCEANS 2011 - IEEE Conference proceedings, Santander, 2011.

[13] H. Hobæk, T. L. Nesse: Scattering from spheres and cylinders - revisited. – In: Proc. 29^{th} Scandinavian Symposium on Physical Acoustics, Ustaoset. R. Korneliussen (ed.). Norwegian Physical Society, 29. January–1. February 2006, ISBN 82–813–001–0.

[14] F. Sigworth. http://www.mathworks.com/matlabcentral/fileexchange/4317-state-machine-simplex-minimizer.

[15] J. Newton, C. L. Wilson: Metallurgy of copper. J. Wiley & Sons Inc, 1942.

[16] D. Gerlich, G. C. Kennedy: Elastic moduli and their pressure derivates for tungsten carbide with different amounts of cobalt binder. J. Appl. Physics **50** (1979) 3331–3333.

[17] A. Islas-Cital, P. R. Atkins, K. Y. Foo: Standard target calibration of broad-band active sonar systems in a laboratory tank. OCEANS 2010 - IEEE Conference Proceedings, Sydney, 2010.

[18] K. G. Foote: Maintaining precision calibrations with optimal copper spheres. J. Acoust. Soc. America **73** (1983) 1054–1063.

Document downloaded by @DAEL, 2026-11-15 00:34:39 - personal use only